Journal of Biomechanics 101 (2020) 109648

Contents lists available at ScienceDirect

Journal of Biomechanics

journal homepage: www.elsevier.com/locate/jbiomech
www.JBiomech.com

A multiscale framework for evaluating three-dimensional cell mechanics in fibril-reinforced poroelastic tissues with anatomical cell distribution – Analysis of chondrocyte deformation behavior in mechanically loaded articular cartilage

Petri Tanska [a,*], Mikko S Venäläinen [a,b], Ahmet Erdemir [c], Rami K Korhonen [a]

[a] Department of Applied Physics, University of Eastern Finland, Kuopio, Finland
[b] Turku Bioscience Centre, University of Turku, Turku and Åbo Akademi University, Turku, Finland
[c] Deparment of Biomedical Engineering, Lerner Research Institute, Cleveland Clinic, Cleveland, USA

ARTICLE INFO

Article history:
Accepted 16 January 2020

Keywords:
Articular cartilage
Finite element analysis
Collagen
Chondrocyte
Poroelastic
Fibril-reinforced
Cell mechanics

ABSTRACT

Characterization of the mechanical environment of cells in collagenous biological tissues during different daily activities is crucial for understanding the role of mechanics on cell biosynthesis and tissue health. However, current imaging methods are limited in characterizing very fast deformations of cells. This could be achieved with computational multiscale modeling, but current models accommodating collagen fibril networks and poroelastic ground matrix have included only a single cell. In this study, a workflow was developed for generating a three-dimensional multiscale model with imaging-based anatomical cell distributions and their micro-environment (pericellular and extracellular matrix). Fibril-reinforced poroelastic material models with (FRPES) and without (FRPE) swelling were implemented into the model and simulations were performed for evaluating cell deformations before and after experimental loading conducted for rabbit knee joint cartilage. We observed that the cells experienced considerably different deformation based on their location in all models. Both FRPE and FRPES models were able to predict the trends in the changes in cell deformations, although the average and median magnitudes differed between the model predictions and experiments. However, the FRPES model results were generally closer to the experimental results. Current findings suggest that morphological properties of cells are affected by the variations in the tissue properties between the samples and variations within the sample caused by the measurement geometry, local structure and composition. Thus, it would be important to consider the anatomical distribution and location of multiple cells along with the structure of fibril networks if cell deformation metrics are evaluated in collagenous tissues.

1. Introduction

Cells experience different kinds of mechanical loading during daily activities in biological tissues. In articular cartilage, tissue deformation and mechanical signals affect chondrocyte (cartilage cell) function and the onset and progression of osteoarthritis (OA) (Grodzinsky et al., 2000; Guilak et al., 2018). Confocal laser scanning microscopy (Bush and Hall, 2005; Han et al., 2009; Youn et al., 2006), dual photon microscopy (Abusara et al., 2016; Moo et al., 2013) and, recently, micro-computed tomography (μCT) (Kestilä et al., 2017) have been used for *in situ* or *in vivo* imaging of chondrocytes or chondrons. With these methods, cell or chondron imaging is even possible when simultaneous deformation is applied. Yet, these imaging methods can only provide "snapshots" of the tissue deformation, as they are limited by image acquisition time.

These limitations can be circumvented by using computational multiscale modeling approaches for evaluation of mechanical responses of chondrocytes and local tissue. Several investigators have focused on cell mechanics in cartilage and other cartilaginous tissues (Gao et al., 2016; Guilak and Mow, 2000; Gupta and Donahue, 2006; Korhonen et al., 2015; Likhitpanichkul et al., 2005; Moo et al., 2014; Tanska et al., 2015) utilizing multiscale modeling. In these approaches, the cell scale model is often constructed using a fibril-reinforced poroelastic material description which accounts for the time-dependent mechanical response,

* Corresponding author at: Department of Applied Physics, University of Eastern Finland, POB 1627, FI-70211 Kuopio, Finland.
E-mail address: petri.tanska@uef.fi (P. Tanska).

https://doi.org/10.1016/j.jbiomech.2020.109648
0021-9290/

collagen network structure and some models even consider tissue swelling. However, those models include only a few cells, thus, they may not fully reflect the true mechanical environment of cells.

Recently, Bennetts et al. (2015) proposed an automated method for generating three-dimensional (3-D) meshes with ellipsoidal cellular and pericellular inclusions using a porous hyperelastic material. If this method would be combined with the segmentation of cell imaging data and fibril-reinforced poroelastic material model, it would allow accounting the effect of cell distribution in the models. This could improve the detail and accuracy of our models in characterizing local cell deformation, stresses and strains in the fibrous tissue matrix, which may improve our understanding of mechanical cell-matrix interactions in connective tissues.

Thus, our aim was to combine present cell segmentation and meshing workflows and fibril-reinforced poroelastic material description to consider the effect of physiological cell distribution in cartilage. Furthermore, we conducted a parametric investigation to quantify which properties of the model are the most crucial on the cell deformation in fibril-reinforced materials when multiple cells are present. This was conducted due to large variations in the pericellular and cellular properties in the literature. Thus, through simulations, this study provides novel insights on how cartilage cells are responding to the mechanical loading in an individualized manner.

2. Materials and methods

2.1. Cell imaging and segmentation

See Fig. 1 for the workflow of the study. Cell imaging was conducted in an earlier study using confocal microscopy (Korhonen et al., 2010), in which an intact patellar cartilage of a skeletally mature (age 13 months) New Zealand white rabbit was stained with Calcein-AM and imaged. Cell segmentations were conducted using an open source cell segmentation software pyCellAnalyst (v1.1.0, http://pycellanalyst.readthedocs.io/; https://github.com/siboles/pyCellAnalyst/, python version 2.7.15). For further details related to cell imaging and segmentation, see supplementary material.

2.2. Material model

There are several fibril-reinforced poroelastic material formulations for modeling cartilaginous tissues (Ateshian et al., 2009; Pierce et al., 2012). In this study, the constitutive model was based on a fibril-reinforced poroelastic material (FRPE) or FRPE material with Donnan osmotic swelling (FRPES) (Wilson et al., 2005b,a, 2004). Briefly, these material models assume that the material consists of a fluid matrix and a porous solid matrix. The solid matrix consists of a linear elastic fibrillar matrix (*i.e.* collagen network) and a hyperelastic non-fibrillar ground matrix (*i.e.* proteoglycan network).

The total stress tensor of the FRPE material is a sum of the individual stress tensors of the tissue constituents (collagen, proteoglycans and fluid):

$$\boldsymbol{\sigma}_{\mathrm{tot,FRPE}} = \sum_{i=1}^{totf} \boldsymbol{\sigma}_{\mathrm{f},i} + \boldsymbol{\sigma}_{\mathrm{nf}} - p\mathbf{I}, \quad (1)$$

where *totf* is the total number of fibrils, $\boldsymbol{\sigma}_{\mathrm{f},i}$ is the stress tensor of a fibril i, $\boldsymbol{\sigma}_{\mathrm{f},i}$ is the stress tensor of the non-fibrillar matrix, p is the fluid pressure and $\mathbf{I}$ is the unit tensor. Similarly, the total stress tensor of the FRPES material is a sum of the individual stress tensors

$$\boldsymbol{\sigma}_{\mathrm{tot,FRPES}} = \sum_{i=1}^{totf} \boldsymbol{\sigma}_{\mathrm{f},i} + \boldsymbol{\sigma}_{\mathrm{nf}} - \Delta\pi\mathbf{I} - \mu_{\mathrm{f}}\mathbf{I} + T_{\mathrm{c}}\mathbf{I}, \quad (2)$$

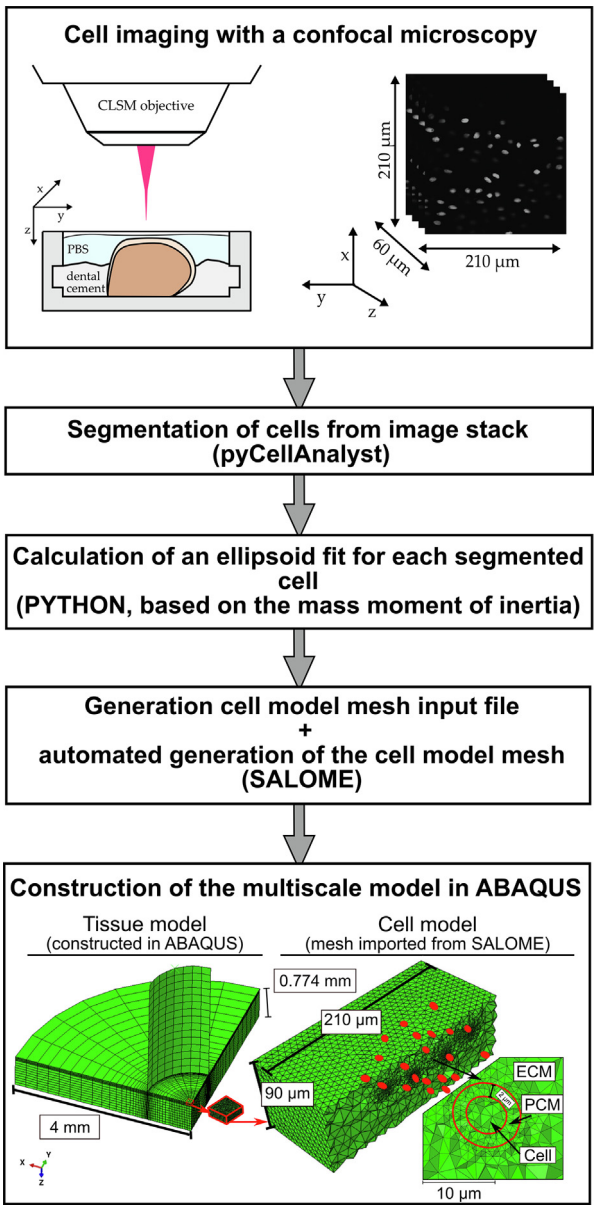

Fig. 1. Overview of the workflow of the study. Cells were imaged using a confocal laser scanning microscope followed by pre-processing in ImageJ (attenuation correction, selection of regions of interest (ROI)). Then, selected ROIs were segmented using pyCellAnalyst and stereolithography (.stl) surfaces were generated. Segmentations were then converted to best-fit ellipsoids by a Python script which utilized a mass moment of inertia and assumed a uniform density for each cell. This ellipsoid fit information (*i.e.* coordinates of cell center and orientation and lengths of principal axes of the ellipsoid) was then used as an input for automated generation of cell model mesh with SALOME (see Bennetts et al., (2015) for more details). Finally, universal mesh file format (.unv) generated by the script was converted to ABAQUS input file format (.inp) and the cell model mesh was imported into ABAQUS followed by the generation of the tissue and cell level models.

where $\Delta\pi$ is the swelling pressure gradient, μ_{f} is the electrochemical potential of water and T_{c} is the chemical expansion stress. See supplementary material for more details.

2.3. Model generation, implementation and boundary conditions

2.3.1. Tissue level model

A 3-D finite-element (FE) tissue model representing patellar cartilage was constructed in indentation geometry using Abaqus/CAE (v. 6.14, Dassault Systémes, USA). Only a quarter of the tissue

was modeled due to the assumed symmetry near the indentation site (Fig. 1). Cartilage tissue (*i.e.* the extracellular matrix, ECM) was meshed using linear pore pressure elements (6912 elements, type C3D8P, characteristic element size = 0.122 mm). The topmost central part (a volume of 0.5 × 0.5 × 0.1 mm^3) of the model was meshed with a greater mesh density for better displacement and pore pressure accuracy (approximate element volume 0.038 × 0.038 × 0.017 mm^3). Cartilage was modeled using (1) the FRPE material, (2) the FRPES material and (3) the FRPES material without the chemical expansion stress (see Eq. (2) and Eq. (A.7) from supplementary material). The material model was implemented in Abaqus using the user-defined material script (UMAT) subroutine.

Mechanical material parameters for the ECM were obtained by manually fitting the model force vs. time response to the experimental data (Ronkainen et al., 2019, 2016), *i.e.*, by matching the peak loading pressure (2 MPa at the rate of 10 μm/s) and equilibrium pressure (0.65 MPa). This resulted in the experimentally observed engineering strain (ε_{eng} = 18.3%) in the FE model. The depth-wise collagen network architecture, collagen content and FCD content of rabbit cartilage were also obtained from the same study (Ronkainen et al., 2019). As the depth-dependent fluid fraction was not quantified in that study, it was assumed based on an earlier study (Tanska et al., 2013). Permeability of the ECM was assumed as strain-dependent (van der Voet, 1997). Those material parameters that could not be uniquely determined from experimental data were obtained from previous studies using the mean reported value. See Table 1 for the material properties and supplementary material for the details of the implementation of the collagen network architecture, collagen content and FCD content.

When using the FRPES material, a free-swelling step was simulated prior to a loading protocol step to establish an osmotic swelling equilibrium in the model. All structural and compositional parameters were kept unchanged during the free-swelling step. This was followed by the experimental loading protocol step (*i.e.* 2nd step in the FRPES models and 1st step in the FRPE model). The loading protocol was based on earlier experimental studies and it consisted of an application of 2 MPa load at a speed of 10 μm/s followed by constant displacement for 20 mins (Fick et al., 2016, 2015; Han et al., 2010; Ronkainen et al., 2019, 2016; Turunen et al., 2013). The thickness of cartilage was based on earlier experimental studies using the same rabbit cartilage samples (Fick et al., 2016; Ronkainen et al., 2019, 2016). Nodes at the coordinate x = 0 were fixed at x-direction and nodes at the coordinate y = 0 were fixed in y-direction (symmetry boundary conditions). Underlaying subchondral bone was considered as rigid, thus, bottom nodes representing cartilage-bone interface were fixed in all directions. Free fluid flow (zero pore pressure boundary condition) was allowed through free surfaces, while no fluid flow was allowed through the bone-cartilage interface (Maroudas et al., 1968), symmetry surfaces and cartilage-indenter contact. The contact was simulated by imposing a displacement boundary condition on the nodes under the indenter in compressive direction.

2.3.2. Cell level model

As the segmented cell geometries were difficult to mesh with a good mesh quality, a custom-made Python script was used for calculating ellipsoid fit. The calculation of the fit was based on the mass moment of inertia by assuming a uniform cell density for each cell (Bennetts et al., 2015; Sibole and Erdemir, 2012) (Fig. 1, see supplementary material for the example script). The ellipsoid fit information was used for constructing a cell model mesh in SALOME (v. 6.3.1) with the meshing script described in Bennetts et al. (2015). A download package incorporating the meshing script is freely accessible from the website (https://simtk.org/home/j2c). Each cell was surrounded by a 2 μm thick PCM and chondrons were embedded into the ECM (Youn et al., 2006). The cell model mesh consisted of 558,722 linear tetrahedral elements (30,451, 140,507 and 387,762 elements in the ECM, PCM and cells, respectively). The mesh was imported in Abaqus

Table 1
Material, compositional and structural reference parameters for fibril-reinforced poroelastic (FRPE) and FRPE swelling (FRPES) cartilage. The tissue level model consisted of the extracellular matrix (ECM), while the cell level model consisted of 21 cells, the pericellular matrices (PCM) of the cells and the ECM.

	Reference material parameters						
	FRPE material			FRPES material			
Material parameter	ECM	PCM	Cell	ECM	PCM	Cell	Description
E_f (MPa)	7.0[†]	0.1 × $E_{f,ECM}$[g]	–	1.73[†]	0.1 × $E_{f,ECM}$[g]	–	Fibril network modulus
E_{nf} (MPa)	0.9[†]	0.137[b]	0.0119[c]	0.7[†]	0.137[b]	0.0119[c]	Non-fibrillar matrix modulus
ν_{nf} (–)	0.42[a]	0.3[e]	0.3[c]	0.42[a]	0.3[e]	0.3[c]	Poisson's ratio of the non-fibrillar matrix
k_0 (10^{-15} m^4 N^{-1} s^{-1})	6.0[†]	0.1 × $k_{0,ECM}$[h]	0.0079[c]	2.0[†]	0.1 × $k_{0,ECM}$[h]	0.0079[c]	Initial permeability
M (–)	7.1[a]	–	–	7.1[a]	–	–	Permeability deformation dependency factor
C (–)	12.16[a]	12.16[a]	–	12.16[a]	12.16[a]	–	Ratio of primary to secondary collagen fibrils
Composition							
n_f (–)	0.85–0.15z[a]	0.85–0.15z[a]	0.60[d]	0.85–0.15z[a]	0.85–0.15z[a]	0.60[d]	Fluid fraction
ρ_z (–)	0.67 + 0.66z[e]	0.67 + 0.66z[e]	–	0.67 + 0.66z[e]	0.67 + 0.66z[e]	–	Relative collagen density
c_{FCD} (mEq/ml)	–	–	–	$c_{FCD,ECM}$[††]	1.119 × $c_{FCD,ECM}$[e]	0.08[f]	Fixed charge density
Collagen network orientation	Arcade like[e]	Circumferential[g]	No fibrils	Arcade like[e]	Circumferential[g]	No fibrils	
Superficial zone thickness	0.05h	–	–	0.05h	–	–	
Middle zone thickness	0.09h	–	–	0.09h	–	–	
Deep zone thickness	0.86h	–	–	0.86h	–	–	

[a] (Wilson et al., 2005a).
[b] (Wilusz et al., 2013).
[c] (Florea et al., 2017).
[d] (Guilak et al., 2002; Oswald et al., 2008).
[e] (Ronkainen et al., 2019, 2016).
[f] (Korhonen et al., 2011).
[g] (Poole et al., 1992).
[h] (Guilak et al., 2006).
[†] Obtained through optimizing to peak loading pressure of 2 MPa (at 10 μm/s) and to equilibrium loading pressure of 0.65 MPa as reported in (Ronkainen et al., 2019, 2016).
[††] $c_{FCD,ECM}$ = $-6082.26z^{12}$ + $38077.86z^{11}$ + $105126.85z^{10}$ + $168479.11z^{9}$-$173642.15z^{8}$ + $120504.34z^{7}$-$57337.05z^{6}$ + $18705.45z^{5}$-$4125.12z^{4}$ + $598.92z^{3}$-$55.25z^{2}$ + 3.09z + 0.08 as reported in (Ronkainen et al., 2019). z indicates normalized distance from the cartilage surface (surface = 0, cartilage-bone interface = 1), h indicates cartilage thickness.

and converted to linear tetrahedral pore pressure elements (type C3D4P). The cell centers were located between a depth of 16.6–32.7 μm corresponding to 2.1–4.2% of the normalized cartilage thickness (of the tissue model). The cell model was driven by displacements and pore pressures obtained from the nodal output results of the tissue level model (*SUBMODEL option in Abaqus).

The ECM in the cell level model had the same depth-dependent properties (fluid fraction, collagen architecture, collagen content and FCD content (included in the FRPES models) as well as strain-dependent permeability) as the tissue level model. In the PCM, the collagen fibrils were oriented circumferentially to the cell surface. The fibril network modulus in the PCM was assumed to be 10% of the ECM based on the reported diameter of collagen fibrils in the PCM (type VI) which is approximately 90% less than the diameter of the fibrils in the ECM (type II) (Poole et al., 1992). The fluid fraction and collagen content were assumed the same as in the ECM, while permeability was assumed constant. The FCD content of the PCM was based on the experimentally determined optical density of Safranin-O stained histological sections and it was ~1.119 times greater than that of the ECM (Ronkainen et al., 2019). The cells were modeled using a porohyperelastic material with constant fluid fraction and permeability. The FCD content of the cells was also assumed as constant (Table 1). See Table 1 for material parameters of the ECM, PCM and cells.

2.4. Analysis

Mesh convergence study was conducted by varying the mesh density ~10%. The stresses and strains varied less than 5%, thus, the used mesh was considered converging. The models were solved using soils consolidation analysis in Abaqus/Standard (v. 6.14, implicit time integration). The change in the morphological parameters was calculated in each model based on the relative change between the morphological parameter value before loading and at equilibrium (see supplementary material). The chemical expansion has been suggested to play an important role in cartilage swelling (Lai et al., 1991). However, it has also been suggested that current formulation might not be valid (Huyghe et al., 2010, 2009; Mow et al., 2009), thus we present analyses with and without this term. Finally, the results were compared with earlier experimental rabbit cartilage cell deformation studies (Fick et al., 2016; Ojanen et al., 2019; Turunen et al., 2013).

2.4.1. Parametric studies

We also conducted a parametric study to determine the effect of the main mechanical and compositional parameters on the deformation of chondrocytes. This was done due to large variations in the pericellular and cellular properties in the literature and natural variation in animals. See table 2 for the used parameter ranges. In the FRPE model, we focused on the effect of the mechanical parameters, while in the FRPES model we only focused on the effect of the FCD. In general, the physiological variation in the parameters was accounted for in the parametric analysis (if it is known). For instance, in early OA rabbit patellar cartilage, the FCD of the PCM and ECM of the superficial cartilage has been observed to be approximately 25–30% smaller compared to healthy tissue (Ojanen et al., 2018; Turunen et al., 2013).

In the mechanical properties, the main focus was on the properties of the PCM as it has been suggested to have an important role as a transducer of mechanical signals between the ECM and cell (Guilak et al., 2018; Steward et al., 2013; Zelenski et al., 2015). However, as the collagen network properties of the PCM are not well-known, thus a wide range for the collagen network modulus (up to the modulus of the ECM collagen fibrils) was used in the parametric analysis. In some studies, collagen network properties are assumed to be the same as in the ECM (Khoshgoftar et al., 2017), however, this may not be true as the collagen type is different (PCM: type VI; ECM: type II). Here, we assumed that the collagen network modulus in the PCM was 10% of that in the ECM (Julkunen et al., 2009), which is based on the fibril diameter in the PCM (Poole et al., 1992).

Table 2
Ranges of the material and compositional parameters used in the parametric study. In the fibril-reinforced poroelastic (FRPE) model E_f, E_{nf} and ν of the ECM, PCM and cells were varied. In the FRPE swelling model, ^{c}FCD of the ECM, PCM and cells was the only varied parameter. During the parametric study, the rest of the model parameters were kept at their reference value.

	FRPE material		
Parameter	ECM	PCM	Cell
E_f(MPa)	[4.5–10.5][a,b,c]	[0.07–7.0][b,c,d,e,f,g]	–
E_{nf}(MPa)	–	[0.014–0.21][c,e,f,g]	[0.001–0.023][h,i,j,k,l,m,n]
ν_{nf} (–)	–	[0.15–0.45][†]	[0.01–0.45][h,i,j,k,l,m,n]
	FRPES material		
Parameter	ECM	PCM	Cell
c_{FCD} (mEq/ml)	$c_{FCD,ECM}$[†,††,a,c,o], where β = [0.7, 1, 1.3]	[0.78–1.29] × $c_{FCD,ECM}$[††,b,o]	[0.056–0.10][†,o]

[a] (Tanska et al., 2013).
[b] (Ronkainen et al., 2019).
[c] (Mäkelä et al., 2015).
[d] (Poole et al., 1992).
[e] (Khoshgoftar et al., 2017).
[f] (Wilusz et al., 2013; Wilusz et al., 2014).
[g] (McLeod et al., 2013).
[h] (Chahine et al., 2013).
[i] (Darling et al., 2006).
[j] (Florea et al., 2017).
[k] (Leipzig and Athanasiou, 2005).
[l] (Nguyen et al., 2010).
[m] (Shieh et al., 2006).
[n] (Jones et al., 1999).
[o] (Ojanen et al., 2018).
[†] Variation assumed based on the values reported for the extracellular matrix (superficial zone).
[††] $c_{FCD,ECM} = -6082.26z^{12} + 38077.86z^{11} + 105126.85z^{10} + 168479.11z^{9} - 173642.15z^{8} + 120504.34z^{7} - 57337.05z^{6} + 18705.45z^{5} - 4125.12z^{4} + 598.92z^{3} - 55.25z^{2} + 3.09z + 0.08\beta$.

In the ECM, we focused only on the collagen fibril network modulus, as the collagen fibril network is the main contributor to the mechanical response of the ECM in indentation (Korhonen et al., 2002; Párraga Quiroga et al., 2017). The range for this parameter was based on previous studies of rabbit cartilage (Mäkelä et al., 2015; Tanska et al., 2013). Note that during the parametric analysis of the ECM, the load was kept at 2 MPa.

We also investigated the effect of the non-fibrillar matrix modulus and Poisson's ratio of cells on the chondrocyte deformation due to the high range of reported values for these parameters in the literature (from ~0.1 kPa to 20 kPa and from 0.07 (linear biphasic model fit) to 0.5, respectively (Chahine et al., 2013; Darling et al., 2006; Florea et al., 2017; Leipzig and Athanasiou, 2005; Nguyen et al., 2010; Shieh et al., 2006).

Data processing and analysis were conducted using custom Python scripts and MATLAB (R2017b, The MathWorks, Inc., USA).

2.4.2. Statistical analyses

Statistical analyses were conducted to the outcome variables (cell volume, height, width and depth) to test whether they were (1) different between the material models (FRPE, FRPES and FRPES without eq. (A.7)) or (2) different between the simulations and the experiments. In addition, we tested whether the experimental studies were statistically significant from each other. Prior to the statistical testing, the normality of the data (Shapiro-Wilk) and

equality of variance (Brown-Forsythe) were tested. Based on these prior tests, (1) the comparison between the outcomes of different material models was conducted using a nonparametric dependent-samples one-way analysis of variance (ANOVA) with Tukey's *post hoc* test for multiple comparisons, while (2) the comparison between the outcomes of the models and experiments was conducted using either parametric or non-parametric independent-samples one-way ANOVA with Tukey's (for parametric cases) or Dunn's (for nonparametric cases) *post hoc* tests. The level of significance was set to $\alpha = 0.05$. The statistical analyses were conducted in SigmaPlot (v. 13, Systat Software, Inc., USA).

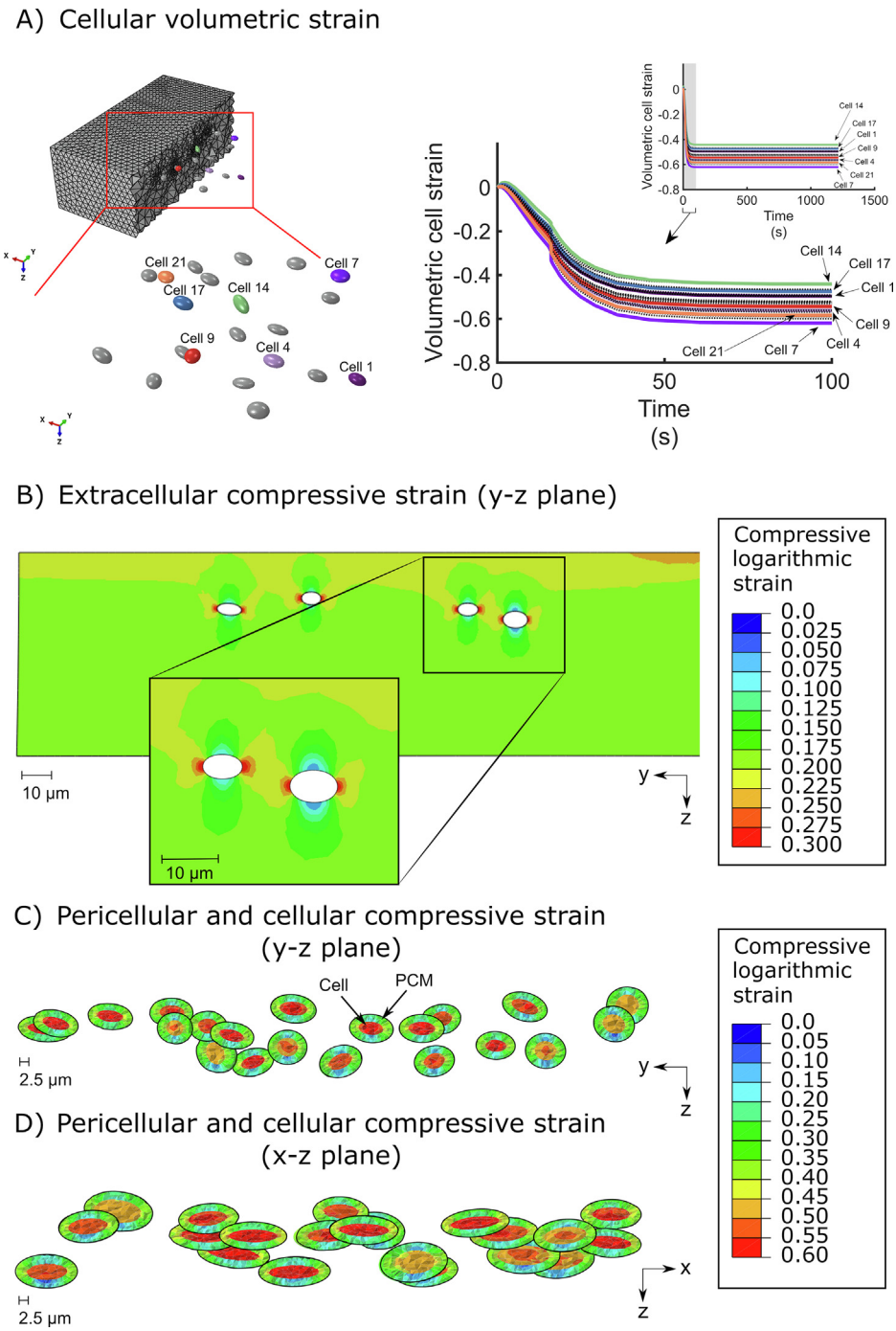

Fig. 2. (a) A visualization of the implemented cell distribution in the cell level model and the simulated cellular volumetric strain during the stress-relaxation of the numbered cells in fibril-reinforced poroelastic cartilage. The volumetric strain was calculated as $\varepsilon_v = (\sum_n V_n)/\left(\sum_n V_n^0\right) - 1$, where V_n is the volume of the element n at the equilibrium and V_n^0 is the volume of the element before loading (Sibole and Erdemir, 2012). Dashed black lines in the strain vs. time graphs show the response of the non-numbered cells. (b) Cross-sectional slice presenting the simulated compressive logarithmic strain distribution of the the extracellular matrix at the equilibrium from y-z plane. For clarity, the pericellular matrices (PCMs) and cells are not shown. (c and d) The simulated compressive logarithmic strain distributions in the PCM and cells at the equilibrium. In these illustrations, each cell is cut in half. In figures b-d, cartilage was modeled using the fibril-reinforced poroelastic swelling material.

3. Results

3.1. Matrix and cell deformation in the FRPE and FRPES models and comparison to the experimental studies

Individual cells experienced different volumetric deformation as a function of the simulated stress-relaxation (Fig. 2a). The volumetric cell deformation of the individual cells reached a steady-state approximately 50 s after the application of the 2 MPa load. The ECM was subjected to a non-uniform strain distribution and the local compressive logarithmic strain values in the cell level model (*i.e.* superficial cartilage) exceeded the engineering strain value (~18.3% which corresponds the logarithmic strain value of ~0.168) of the loading protocol (Fig. 2b). Pericellular and cellular compressive logarithmic strains varied depending on the location and orientation of the cell (Fig. 2cd).

In general, the FRPE model showed significantly greater changes in cell volume, height and depth, while cell width was changed significantly less compared to the FRPES models (Fig. 3 and Table 3). In addition, the FRPES models were not significantly different from each other except in the case of the change in cell width, in which the FRPES model exhibited a slightly greater change in cell width compared to the FRPES model without the chemical expansion stress term.

When the FRPE and FRPES model predictions were compared against the experimentally observed cell deformation (Fick et al., 2016; Ojanen et al., 2019; Turunen et al., 2013), the trend of the change in deformation was consistent with experimental findings, *i.e.*, if volume was decreased in the experiments, it was also decreased in the model (Fig. 3 and Table 3). The only exception was the change in cell width, for which the models predicted a decrease in width following the mechanical loading, while in the experimental studies the width was increased. However, in some cases, the magnitudes of the simulated changes were overestimated when compared to the experiments, *i.e.*, the change in cell volume in the FRPE and FRPES models and the change in cell height in the FRPE model. Importantly, the difference between the predicted changes and experimental data in the FRPES models was dependent on the experimental data. For example, the change in cell height was not different compared to the data presented in Fick et al. (2016).

3.2. Parametric study

Smaller collagen fibril network modulus values in the PCM resulted in greater cell deformation, while smaller non-fibrillar matrix modulus values in the PCM resulted in smaller cell deformation (Fig. 4ab). Likewise, smaller pericellular Poisson's ratio resulted in smaller cell deformation (Fig. 4c). As in the PCM, smaller collagen fibril network modulus values in the ECM resulted in greater cell deformation (Fig. 5). Smaller cellular non-fibrillar matrix modulus resulted in greater cell deformation (Fig. 6a), while smaller cellular Poisson's ratio resulted in greater cell deformation (Fig. 6b). Compared to the reference model, an increase or decrease of the FCD content of the ECM or PCM resulted in smaller cell deformation, although the effect of the FCD of the ECM on cell deformation was smaller than that of the PCM (Fig. 7ab). Further, greater FCD content in cells resulted in smaller cell deformation (Fig. 7c). See supplementary material for more details.

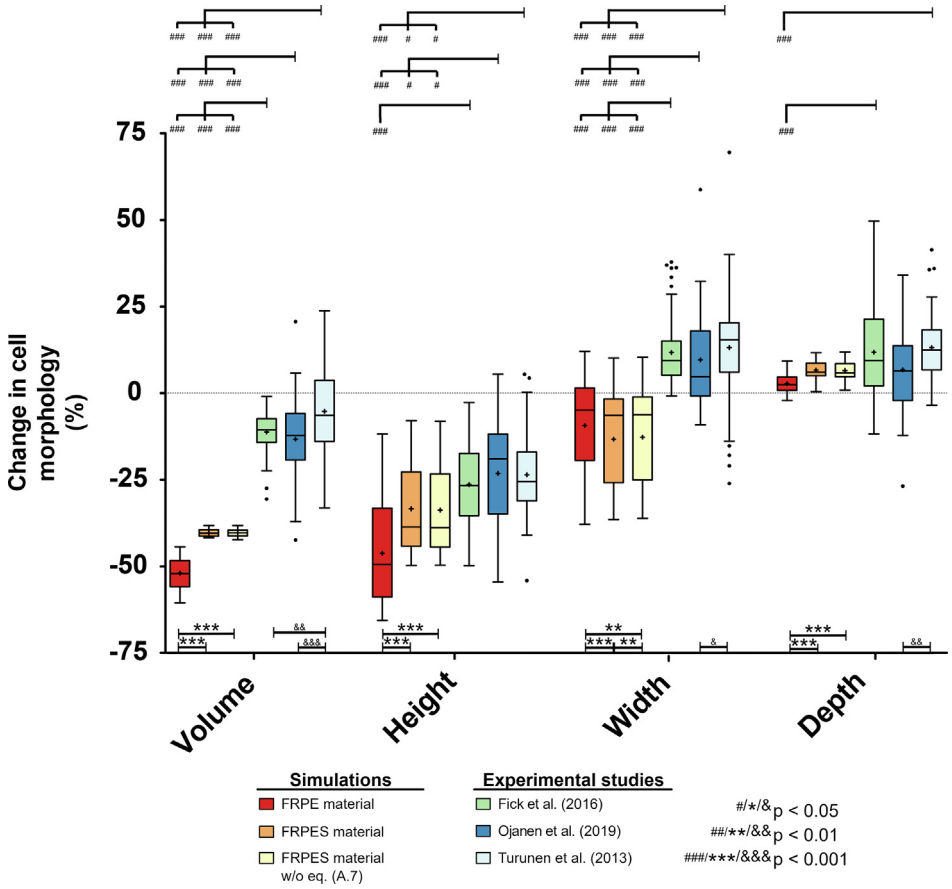

Fig. 3. Simulated and experimentally observed changes in cell volume, height, width and depth due to tissue loading. In the simulations, cartilage tissue was modeled using the fibril-reinforced poroelastic (FRPE) model, the fibril-reinforced poroelastic model with osmotic swelling (FRPES) and the FRPES model without chemical expansion stress (FRPES model w/o eq. (A.7)). The change in parameter = value at steady-state configuration/value at before loading − 1. Boxplot and lines represent median and quartiles; + = mean.

Table 3
Descriptive statistics for the simulated and experimentally observed changes in the morphological parameters of chondrocytes. Simulations and experimental studies use the same loading protocol.

	Simulations			Experiments		
	FRPE material	FRPES material	FRPES material (no eq. A.7)	Fick et al. (2016)	Ojanen et al. (2019)	Turunen et al. (2013)
Number of cells in analysis	21	21	21	90	57	77
Change in cell volume (%)						
Mean ± SD	−51.9 ± 5.0	−40.4 ± 1.0	−40.3 ± 1.0	−11.2 ± 5.8	−13.8 ± 21.3	−5.3 ± 12.5
Median	−52.8	−40.4	−40.3	−10.6	−12.2	−6.6
Min	−60.6	−41.7	−42.3	−30.6	−42.4	−33.1
25% percentile	−55.8	−41.2	−41.2	−14.2	−19.3	−14.0
75% percentile	−48.3	−39.6	−39.6	−7.4	−5.9	3.7
Max	−44.4	−38.2	−38.2	−1.0	20.7	23.8
Change in cell height (%)						
Mean ± SD	−46.3 ± 14.6	−33.4 ± 13.3	−33.7 ± 12.9	−26.4 ± 11.6	−23.3 ± 26.4	−23.5 ± 11.6
Median	−49.5	−38.7	−38.8	−26.7	−19.0	−25.5
Min	−65.6	−49.7	−49.8	−49.8	−54.5	−54.1
25% percentile	−58.8	−44.1	−35.3	−35.3	−34.8	−31.1
75% percentile	−33.2	−22.7	−17.5	−17.5	−11.8	−17.0
Max	−11.8	−8.0	−2.7	−2.7	5.5	5.4
Change in cell width (%)						
Mean ± SD	−9.4 ± 13.7	−13.3 ± 14.5	−12.7 ± 14.4	11.8 ± 13.1	9.5 ± 23.3	13.1 ± 14.3
Median	−4.9	−6.5	−6.2	9.4	4.7	−15.4
Min	−37.9	−36.5	−36.2	−0.8	−9.2	−26.1
25% percentile	−19.4	−25.8	−25.0	5.1	−0.8	6.1
75% percentile	−1.5	−1.7	−1.1	15.0	17.9	20.3
Max	12.0	10.1	10.4	37.9	58.7	70.0
Change in cell depth (%)						
Mean ± SD	2.8 ± 2.7	6.7 ± 2.8	6.5 ± 2.7	11.7 ± 9.2	6.5 ± 16.6	13.1 ± 9.0
Median	2.4	5.0	4.7	2.1	−2.1	12.4
Min	−2.2	0.4	0.9	−11.8	−26.8	−3.5
25% percentile	0.8	5.0	4.7	2.1	−2.1	6.7
75% percentile	4.6	8.7	8.5	21.3	13.7	18.2
Max	9.3	11.7	11.8	49.7	34.0	41.4

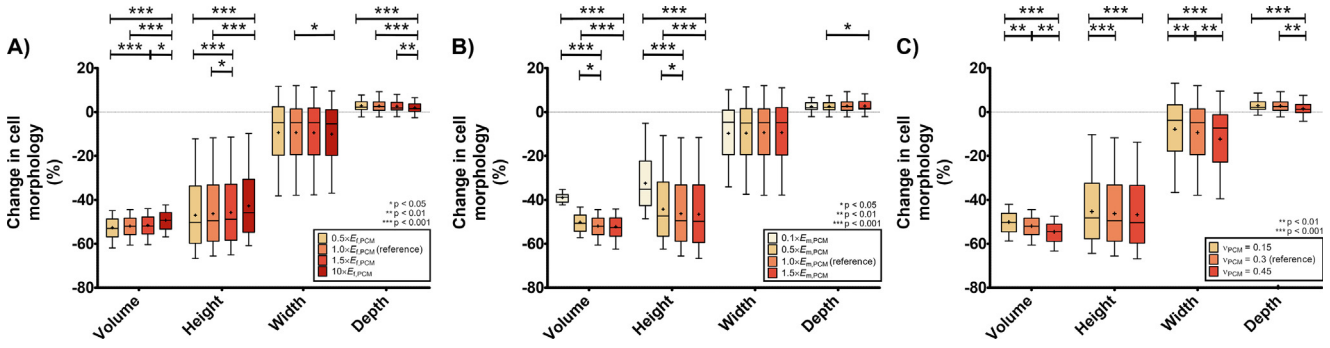

Fig. 4. (a) The effect of the collagen fibril network modulus, (b) the non-fibrillar matrix modulus and (c) the Poisson's ratio of the pericellular matrix (PCM) on the change of cell volume, height, width and depth. Cartilage was modeled using the FRPE material model. The change in parameter = value at steady-state configuration/value at before loading − 1. Boxplot and lines represent median and quartiles; + = mean.

4. Discussion

The multiscale model consisting of tissue and cell levels was created to simulate morphological and volumetric changes of chondrocytes in rabbit patellar cartilage. Cartilage tissue was modeled with fibril-reinforced poro(hyper)elastic material with and without osmotic swelling. The cell level model was based on anatomical cell distribution obtained from confocal microscopy.

We found out that although both fibril-reinforced models were able to simulate similar trends in most of the parameters, namely in the change in cell volume, height and depth (Fig. 3 and Table 3), the model incorporating swelling was closer to the experimentally measured changes. However, in some cases, the mean and median magnitudes of the changes were overestimated when compared to the experiments, *e.g.* in the case of cell volume. This could indicate that the calibration of the mechanical material properties of the ECM was not perfect or the implemented experimental structure and composition might have been different from the true experimental case. It is important to notice that, in the experiments, the changes in cell morphology are sample-specific as the composition and structure typically vary between samples. In the model, this was not fully accounted for as the structure and composition were implemented using an average depth-wise profile obtained from 10 rabbit patellae. Further, the current implementations of structure and composition were based on 2-D analysis (and the split-line orientation was assumed). This means that our implemented structure was a 2-D ensemble from the true 3-D structure and composition. Thus, we might not capture small local variations

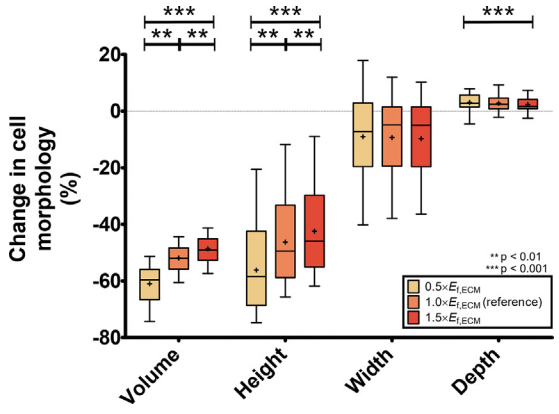

Fig. 5. The effect of the collagen fibril network modulus of the extracellular matrix (ECM) on the change of cell volume, height, width and depth. Cartilage was modeled using the FRPE material model. The change in parameter = value at steady-state configuration/value at before loading − 1. Boxplot and lines represent median and quartiles; + = mean.

in the tissue. These simplifications in the implementation may explain some of the observed differences between the simulated and measured cell deformation parameters. However, we want to emphasize that the experimental results (see Fig. 3 and Table 3) also have large variations, which are most likely due to compositional and structural differences between the measured samples and animals even though the properties of rabbit cartilage should be approximately same (same age (~13 months), same location (patella) and healthy tissue). Yet, collagen architecture and compositional properties should be quantified (and implemented) in a true 3-D manner, and we will investigate this in the future.

A very important finding of this study was that the individual cells did not deform in a similar manner (see Fig. 2). Instead, the cell deformation was dependent on the cell location and this location-dependent deformation is caused by collagen architecture and testing geometry, thus, it would be important to analyze the same cell in experiments to improve the accuracy and precision of the analysis. Further, earlier computational studies with single cells have shown that depth-dependent collagen architecture and matrix composition may have a substantial contribution to the local cell deformation (Korhonen et al., 2008; Ronkainen et al., 2019). We observed that both the indentation geometry and the depth-dependent collagen architecture with split-lines cause a non-uniform strain and stress distribution to the sample, thus, cells experience different deformation. For instance, cartilage matrix was able to expand more in the direction perpendicular to the split-lines. Thus, the split-line orientation modulated the volumetric deformation of the cells; the location of the cells perpendicular to split-line direction correlated with the volumetric deformation (Pearson's r = 0.67, p = 0.001), while the location of the cells along the split-line direction did not correlate with the deformation (r = -0.02, p = 0.92). Interestingly, the volumetric strain did not correlate with tissue depth (r = 0.05, p = 0.82), probably as the cells were located at a relatively thin layer corresponding to 2.1–4.2% of the normalized cartilage thickness (tissue depth 16.6–32.7 μm from the surface). Thus, the depth-wise properties do not change enough to affect depth-wise strain and stress distributions. By obtaining the cells from such a thin layer we were able to optimize

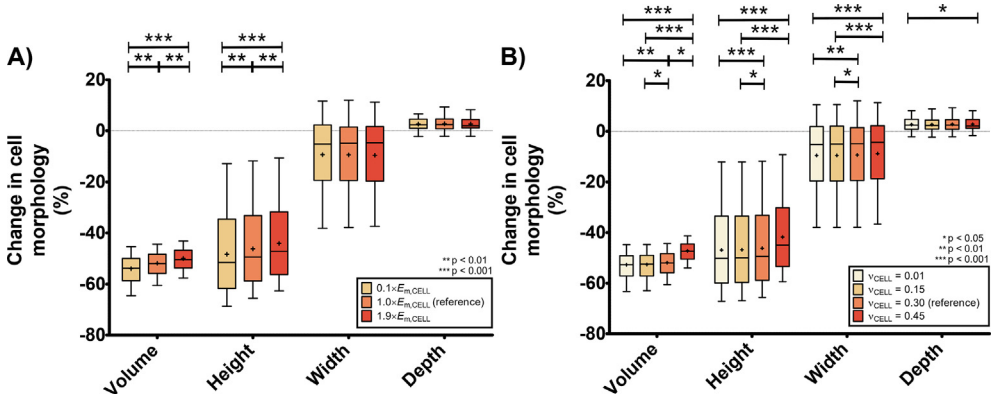

Fig. 6. (a) The effect of the non-fibrillar matrix modulus (*i.e.* Young's modulus) and (b) the Poisson's ratio of the chondrocyte on the change of cell volume, height, width and depth. Cartilage was modeled using the FRPE material model. The change in parameter = value at steady-state configuration/value at before loading − 1. Boxplot and lines represent median and quartiles; + = mean.

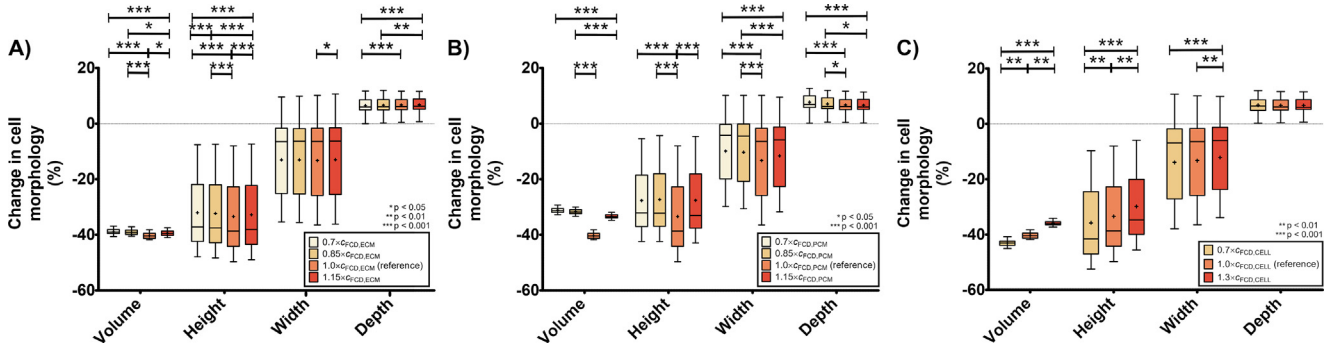

Fig. 7. (a) The effect of the fixed charge density (FCD) distribution of the extracellular matrix (ECM), (b) the pericellular matrix (PCM) and (c) cells on the change of cell volume, height, width and depth. Cartilage was modeled using the FRPES material model. The change in parameter = value at steady-state configuration/value at before loading − 1. Boxplot and lines represent median and quartiles; + = mean.

the signal-to-noise ratio and the quality of cell segmentations. Further, similar analysis depth has also been used in the experimental studies (e.g. in Turunen et al. (2013) analysis depth was ~ 20 μm). Please see supplementary material for further discussion on the limitations of the study.

4.1. Parametric study

The parametric study revealed that the non-fibrillar matrix modulus of the PCM, the collagen fibril network modulus of the ECM, and the FCD of the PCM in the swelling model had the greatest effect on the average and median changes in cell deformation. Further, the FCD content of the cell also modulated cell deformation, while the FCD content of the ECM did not have as a large effect. Interestingly, the FCD content of the PCM modulated cell deformation in a non-linear manner; cell deformation was the greatest at the reference FCD content, while cells deformed less when the FCD of the PCM was either greater or smaller. One possible explanation for this could be that as the FCD of the PCM decreases, the cell with greater FCD content is stiffer relative to the PCM. Thus, the cell can expand inside the PCM and the cell deforms less. Similarly, when the FCD content of the PCM increases, the PCM is stiffer and it can "shield" the cell from excessive deformation. These findings further emphasize the complex role of the PCM in modulating cell deformation and function (Guilak et al., 2018; Zelenski et al., 2015).

The collagen fibril network modulus and the Poisson's ratio of the PCM had a small effect on the changes in cell deformation suggesting that these parameters also have some contribution on cell deformation. Likewise, Young's modulus and Poisson's ratio of the cells had also a small effect on the average and median changes in the cell shape and volume. This would suggest that although the mechanical properties of the chondrocyte do affect the mechanical response of cells, their contribution is smaller than the properties of the PCM or ECM, at least in healthy cartilage.

In summary, we presented a framework for creating a multiscale finite-element model with imaging-based anatomical cell distribution and fibril-reinforced poroelastic material allowing mechanical analysis of cell-matrix interactions of multiple cells. This model may provide new insights related to cell mechanotransduction in fibrous tissues. The results emphasize that cell deformation is affected by the variations in the tissue properties between the samples and variations within the sample caused by the measurement geometry, local structure and composition. These would suggest that it is important to track the same cells in experiments and that cell shape and volume analyses in fibrous tissues should be made from the same locations in order to make valid comparisons.

5. Role of the funding source

The research leading to these results has received funding from the European Research Council under the European Union's Seventh Framework Programme (FP/2007–2013), ERC Grant Agreement no. 281180, the Academy of Finland (#286526, #324529), Research Committee of the Kuopio University Hospital Catchment Area for the State Research Funding (#5654176), Sigrid Juselius Foundation, Finnish Cultural Foundation North Savo regional fund (#65142194, #65161575), Orthopaedic Research Society 2015/2016 Collaborative Exchange Grant and Alfred Kordelin Foundation (#150465). The funding sources had no role in the study design, collection, analysis and interpretation of data; in the writing of the manuscript; and in the decision to submit the manuscript for publication.

CRediT authorship contribution statement

Petri Tanska: Conceptualization, Methodology, Software, Validation, Formal analysis, Investigation, Writing - original draft, Writing - review & editing, Visualization, Project administration, Funding acquisition. **Mikko S Venäläinen:** Software, Validation, Writing - review & editing, Funding acquisition. **Ahmet Erdemir:** Conceptualization, Methodology, Resources, Writing - review & editing. **Rami K Korhonen:** Conceptualization, Methodology, Investigation, Resources, Writing - review & editing, Supervision, Project administration, Funding acquisition.

Declaration of Competing Interest

The authors declare that they have no known competing financial interests or personal relationships that could have appeared to influence the work reported in this paper.

Acknowledgments

CSC—IT Center for Science Ltd., Finland is acknowledged for providing modeling software. Santtu Mikkonen, Ph.D., is acknowledged for statistical consultation and Scott Sibole, M.Sc., for technical support and useful discussions on pyCellAnalyst software. Cristina Florea, Ph.D., is acknowledged for linguistic comments. Ari Ronkainen, Ph.D., James Fick, Ph.D., Simo Ojanen, M.Sc., and Siru Kaartinen née Turunen, Ph.D., are acknowledged for providing experimental cell morphology data. The authors want also to thank members of the Erdemir laboratory for useful discussions.

Appendix A. Supplementary material

Supplementary data to this article can be found online at https://doi.org/10.1016/j.jbiomech.2020.109648.

References

Abusara, Z., Von Kossel, M., Herzog, W., 2016. In vivo dynamic deformation of articular cartilage in intact joints loaded by controlled muscular contractions. PLoS ONE 11,. https://doi.org/10.1371/journal.pone.0147547 e0147547.

Ateshian, G.A., Costa, K.D., Azeloglu, E.U., Morrison, B., Hung, C.T., 2009. Continuum modeling of biological tissue growth by cell division, and alteration of intracellular osmolytes and extracellular fixed charge density. J. Biomech. Eng. 131. https://doi.org/10.1115/1.3192138.

Bennetts, C.J., Sibole, S., Erdemir, A., 2015. Automated generation of tissue-specific three-dimensional finite element meshes containing ellipsoidal cellular inclusions. Comput. Methods Biomech. Biomed. Eng. 18, 1293–1304. https://doi.org/10.1080/10255842.2014.900545.

Bush, P.G., Hall, A.C., 2005. Passive osmotic properties of in situ human articular chondrocytes within non-degenerate and degenerate cartilage. J. Cell. Physiol. 204, 309–319. https://doi.org/10.1002/jcp.20294.

Chahine, N.O., Blanchette, C., Thomas, C.B., Lu, J., Haudenschild, D., Loots, G.G., 2013. Effect of age and cytoskeletal elements on the indentation-dependent mechanical properties of chondrocytes. PLoS ONE 8,. https://doi.org/10.1371/journal.pone.0061651 e61651.

Darling, E.M., Zauscher, S., Guilak, F., 2006. Viscoelastic properties of zonal articular chondrocytes measured by atomic force microscopy. Osteoarthr. Cartil. 14, 571–579. https://doi.org/10.1016/j.joca.2005.12.003.

Fick, J.M., Ronkainen, A., Herzog, W., Korhonen, R.K., 2015. Site-dependent biomechanical responses of chondrocytes in the rabbit knee joint. J. Biomech. 48, 4010–4019. https://doi.org/10.1016/j.jbiomech.2015.09.049.

Fick, J.M., Ronkainen, A.P., Madden, R., Sawatsky, A., Tiitu, V., Herzog, W., Korhonen, R.K., 2016. Early in situ changes in chondrocyte biomechanical responses due to a partial meniscectomy in the lateral compartment of the mature rabbit knee joint. J. Biomech. 49, 4057–4064. https://doi.org/10.1016/j.jbiomech.2016.10.039.

Florea, C., Tanska, P., Mononen, M.E., Qu, C., Lammi, M.J., Laasanen, M.S., Korhonen, R.K., 2017. A combined experimental atomic force microscopy-based nanoindentation and computational modeling approach to unravel the key contributors to the time-dependent mechanical behavior of single cells. Biomech. Model. Mechanobiol. 16, 297–311. https://doi.org/10.1007/s10237-016-0817-y.

Gao, X., Zhu, Q., Gu, W., 2016. Prediction of glycosaminoglycan synthesis in intervertebral disc under mechanical loading. J. Biomech. 49, 2655–2661. https://doi.org/10.1016/j.jbiomech.2016.05.028.
Grodzinsky, A.J., Levenston, M.E., Jin, M., Frank, E.H., 2000. Cartilage tissue remodeling in response to mechanical forces. Annu. Rev. Biomed. Eng. 2, 691–713. https://doi.org/10.1146/annurev.bioeng.2.1.691.
Guilak, F., Alexopoulos, L.G., Upton, M.L., Youn, I., Choi, J.B., Cao, L., Setton, L.A., Haider, M.A., 2006. The pericellular matrix as a transducer of biomechanical and biochemical signals in articular cartilage. Ann. N. Y. Acad. Sci. 1068, 498–512. https://doi.org/10.1196/annals.1346.011.
Guilak, F., Erickson, G.R., Ting-Beall, H.P., 2002. The effects of osmotic stress on the viscoelastic and physical properties of articular chondrocytes. Biophys. J. 82, 720–727. https://doi.org/10.1016/S0006-3495(02)75434-9.
Guilak, F., Mow, V.C., 2000. The mechanical environment of the chondrocyte: a biphasic finite element model of cell-matrix interactions in articular cartilage. J. Biomech. 33, 1663–1673. https://doi.org/10.1016/S0021-9290(00)00105-6.
Guilak, F., Nims, R.J., Dicks, A., Wu, C.-L., Meulenbelt, I., 2018. Osteoarthritis as a disease of the cartilage pericellular matrix. Matrix Biol. https://doi.org/10.1016/j.matbio.2018.05.008.
Gupta, T., Donahue, T.L.H., 2006. Role of cell location and morphology in the mechanical environment around meniscal cells. Acta Biomater. 2, 483–492. https://doi.org/10.1016/j.actbio.2006.05.009.
Han, S.-K., Colarusso, P., Herzog, W., 2009. Confocal microscopy indentation system for studying in situ chondrocyte mechanics. Med. Eng. Phys. 31, 1038–1042. https://doi.org/10.1016/j.medengphy.2009.05.013.
Han, S.-K., Seerattan, R., Herzog, W., 2010. Mechanical loading of in situ chondrocytes in lapine retropatellar cartilage after anterior cruciate ligament transection. J. R. Soc. Interface 7, 895–903. https://doi.org/10.1098/rsif.2009.0458.
Huyghe, J.M., Wilson, W., Malakpoor, K., 2010. Reply to discussion: "On the thermodynamical admissibility of the triphasic theory of charged hydrated tissues" (Mow, V. C., Lai, W. M., Setton, L. A., Gu, W., Yao, H., and Lu, X. L., 2009, ASME J. Biomech. Eng., 131, p. 095501). J. Biomech. Eng. 132, 065501. https://doi.org/10.1115/1.4001076.
Huyghe, J.M., Wilson, W., Malakpoor, K., 2009. On the thermodynamical admissibility of the triphasic theory of charged hydrated tissues. J. Biomech. Eng. 131,. https://doi.org/10.1115/1.3049531 044504.
Jones, W.R., Ting-Beall, H.P., Lee, G.M., Kelley, S.S., Hochmuth, R.M., Guilak, F., 1999. Alterations in the Young's modulus and volumetric properties of chondrocytes isolated from normal and osteoarthritic human cartilage. J. Biomech. 32, 119–127. https://doi.org/10.1016/s0021-9290(98)00166-3.
Julkunen, P., Wilson, W., Jurvelin, J.S., Korhonen, R.K., 2009. Composition of the pericellular matrix modulates the deformation behaviour of chondrocytes in articular cartilage under static loading. Med. Biol. Eng. Comput. 47, 1281–1290. https://doi.org/10.1007/s11517-009-0547-8.
Kestilä, I., Thevenot, J.P., Finnilä, M.A., Karhula, S.S., Hadjab, I., Kauppinen, S., Garon, M., Quenneville, E., Rieppo, L., Pritzker, K.P., Buschmann, M.D., Nieminen, H.J., Saarakkala, S., 2017. Automatic 3D selection, segmentation, and analysis of human articular cartilage Chondrons from micro-computed tomography in vitro. Osteoarthr. Cartil. 25, S321. https://doi.org/10.1016/j.joca.2017.02.538.
Khoshgoftar, M., Torzilli, P.A., Maher, S.A., 2017. Influence of the pericellular and extracellular matrix structural properties on chondrocyte mechanics. J. Orthop. Res. 1, 1–9. https://doi.org/10.1002/jor.23774.
Korhonen, R., Wong, M., Arokoski, J., Lindgren, R., Helminen, H., Hunziker, E., Jurvelin, J., 2002. Importance of the superficial tissue layer for the indentation stiffness of articular cartilage. Med. Eng. Phys. 24, 99–108. https://doi.org/10.1016/S1350-4533(01)00123-0.
Korhonen, R.K., Han, S.-K., Herzog, W., 2010. Osmotic loading of articular cartilage modulates cell deformations along primary collagen fibril directions. J. Biomech. 43, 783–787. https://doi.org/10.1016/j.jbiomech.2009.10.022.
Korhonen, R.K., Julkunen, P., Jurvelin, J.S., Saarakkala, S., 2011. Structural and compositional changes in Peri- and extracellular matrix of osteoarthritic cartilage modulate chondrocyte morphology. Cell. Mol. Bioeng. 4, 484–494. https://doi.org/10.1007/s12195-011-0178-7.
Korhonen, R.K., Julkunen, P., Wilson, W., Herzog, W., 2008. Importance of collagen orientation and depth-dependent fixed charge densities of cartilage on mechanical behavior of chondrocytes. J. Biomech. Eng. 130,. https://doi.org/10.1115/1.2898725 021003.
Korhonen, R.K., Tanska, P., Kaartinen, S.M., Fick, J.M., Mononen, M.E., 2015. New concept to restore normal cell responses in osteoarthritic knee joint cartilage. Exerc. Sport Sci. Rev. 43, 143–152. https://doi.org/10.1249/JES.0000000000000051.
Lai, W.M., Hou, J.S., Mow, V.C., 1991. A triphasic theory for the swelling and deformation behaviors of articular cartilage. J. Biomech. Eng. 113, 245–258.
Leipzig, N.D., Athanasiou, K.A., 2005. Unconfined creep compression of chondrocytes. J. Biomech. 38, 77–85. https://doi.org/10.1016/j.jbiomech.2004.03.013.
Likhitpanichkul, M., Guo, X.E., Mow, V.C., 2005. The effect of matrix tension-compression nonlinearity and fixed negative charges on chondrocyte responses in cartilage. Mol. Cell. Biomech. 2, 191–204.
Mäkelä, J.T.A., Han, S.-K., Herzog, W., Korhonen, R.K., 2015. Very early osteoarthritis changes sensitively fluid flow properties of articular cartilage. J. Biomech. 48, 3369–3376. https://doi.org/10.1016/j.jbiomech.2015.06.010.
Maroudas, A., Bullough, P., Swanson, S.A., Freeman, M.A., 1968. The permeability of articular cartilage. J. Bone Joint Surg. Br. 50, 166–177.
McLeod, M.A., Wilusz, R.E., Guilak, F., 2013. Depth-dependent anisotropy of the micromechanical properties of the extracellular and pericellular matrices of articular cartilage evaluated via atomic force microscopy. J. Biomech. 46, 586–592. https://doi.org/10.1016/j.jbiomech.2012.09.003.
Moo, E.K., Abusara, Z., Abu Osman, N.A., Pingguan-Murphy, B., Herzog, W., 2013. Dual photon excitation microscopy and image threshold segmentation in live cell imaging during compression testing. J. Biomech. 46, 2024–2031. https://doi.org/10.1016/j.jbiomech.2013.06.007.
Moo, E.K., Han, S.K., Federico, S., Sibole, S.C., Jinha, A., Abu Osman, N.A., Pingguan-Murphy, B., Herzog, W., 2014. Extracellular matrix integrity affects the mechanical behaviour of in-situ chondrocytes under compression. J. Biomech. 47, 1004–1013. https://doi.org/10.1016/j.jbiomech.2014.01.003.
Mow, V.C., Michael Lai, W., Setton, L.A., Gu, W., Yao, H., Wan, L.Q., Lu, X.L., 2009. Discussion: "On the Thermodynamical Admissibility of the Triphasic Theory of Charged Hydrated Tissues" (Huyghe, J. M., Wilson, W., and Malakpoor, K., ASME J. Biomech. Eng., 2009, 131, p. 044504). J. Biomech. Eng. 131, 095501. https://doi.org/10.1115/1.3128727.
Nguyen, B.V., Wang, Q.G., Kuiper, N.J., El Haj, A.J., Thomas, C.R., Zhang, Z., 2010. Biomechanical properties of single chondrocytes and chondrons determined by micromanipulation and finite-element modelling. J. R. Soc. Interface 7, 1723–1733. https://doi.org/10.1098/rsif.2010.0207.
Ojanen, S.P., Finnilä, M.A.J., Mäkelä, J.T.A., Saarela, K., Happonen, E., Herzog, W., Saarakkala, S., Korhonen, R.K., 2019. Anterior cruciate ligament transection of rabbits alters composition, structure and biomechanics of articular cartilage and chondrocyte deformation 2 weeks post-surgery in a site-specific manner. J. Biomech. 109450. https://doi.org/10.1016/j.jbiomech.2019.109450.
Ojanen, S.P., Finnilä, M.A.J., Reunamo, A.E., Ronkainen, A.P., Mikkonen, S., Herzog, W., Saarakkala, S., Korhonen, R.K., 2018. Site-specific glycosaminoglycan content is better maintained in the pericellular matrix than the extracellular matrix in early post-traumatic osteoarthritis. PLoS ONE 13,. https://doi.org/10.1371/journal.pone.0196203 e0196203.
Oswald, E.S., Chao, P.G., Bulinski, J.C., Ateshian, G.A., Hung, C.T., 2008. Dependence of zonal chondrocyte water transport properties on osmotic environment. Cell. Mol. Bioeng. 1, 339–348. https://doi.org/10.1007/s12195-008-0026-6.
Párraga Quiroga, J.M., Wilson, W., Ito, K., van Donkelaar, C.C., 2017. Relative contribution of articular cartilage's constitutive components to load support depending on strain rate. Biomech. Model. Mechanobiol. 16, 151–158. https://doi.org/10.1007/s10237-016-0807-0.
Pierce, D.M., Ricken, T., Holzapfel, G.A., 2012. A hyperelastic biphasic fibre-reinforced model of articular cartilage considering distributed collagen fibre orientations: continuum basis, computational aspects and applications. Comput. Methods Biomech. Biomed. Eng. 5842, 1–18. https://doi.org/10.1080/10255842.2012.670854.
Poole, C.A., Ayad, S., Gilbert, R.T., 1992. Chondrons from articular cartilage. V. Immunohistochemical evaluation of type VI collagen organisation in isolated chondrons by light, confocal and electron microscopy. J. Cell Sci. 103 (Pt 4), 1101–1110.
Ronkainen, A.P., Fick, J.M., Herzog, W., Korhonen, R.K., 2016. Site-specific cell-tissue interactions in rabbit knee joint articular cartilage. J. Biomech. 49, 2882–2890. https://doi.org/10.1016/j.jbiomech.2016.06.033.
Ronkainen, A.P., Tanska, P., Fick, J.M., Herzog, W., Korhonen, R.K., 2019. Interrelationship of cartilage composition and chondrocyte mechanics after a partial meniscectomy in the rabbit knee joint – experimental and numerical analysis. J. Biomech. 83, 65–75. https://doi.org/10.1016/j.jbiomech.2018.11.024.
Shieh, A.C., Koay, E.J., Athanasiou, K.A., 2006. Strain-dependent recovery behavior of single chondrocytes. Biomech. Model. Mechanobiol. 5, 172–179. https://doi.org/10.1007/s10237-006-0028-z.
Sibole, S.C., Erdemir, A., 2012. Chondrocyte deformations as a function of tibiofemoral joint loading predicted by a generalized high-throughput pipeline of multi-scale simulations. PLoS ONE 7,. https://doi.org/10.1371/journal.pone.0037538 e37538.
Steward, A.J., Wagner, D.R., Kelly, D.J., 2013. The pericellular environment regulates cytoskeletal development and the differentiation of mesenchymal stem cells and determines their response to hydrostatic pressure. Eur. Cell. Mater. 25, 167–178. https://doi.org/vol025a12 [pii].
Tanska, P., Mononen, M.E., Korhonen, R.K., 2015. A multi-scale finite element model for investigation of chondrocyte mechanics in normal and medial meniscectomy human knee joint during walking. J. Biomech. 48, 1397–1406. https://doi.org/10.1016/j.jbiomech.2015.02.043.
Tanska, P., Turunen, S.M., Han, S.K., Julkunen, P., Herzog, W., Korhonen, R.K., 2013. Superficial collagen fibril modulus and pericellular fixed charge density modulate chondrocyte volumetric behaviour in early osteoarthritis. Comput. Math. Methods Med. 2013, 1–14. https://doi.org/10.1155/2013/164146.
Turunen, S.M., Han, S.-K., Herzog, W., Korhonen, R.K., 2013. Cell deformation behavior in mechanically loaded rabbit articular cartilage 4 weeks after anterior cruciate ligament transection. Osteoarthr. Cartilage 21, 505–513. https://doi.org/10.1016/j.joca.2012.12.001.
van der Voet, A., 1997. A comparison of finite element codes for the solution of biphasic poroelastic problems. Proc. Inst. Mech. Eng. H. 211, 209–211. https://doi.org/10.1118/1.597333.
Wilson, W., van Donkelaar, C.C., van Rietbergen, B., Huiskes, R., 2005a. A fibril-reinforced poroviscoelastic swelling model for articular cartilage. J. Biomech. 38, 1195–1204. https://doi.org/10.1016/j.jbiomech.2004.07.003.
Wilson, W., van Donkelaar, C.C., van Rietbergen, B., Ito, K., Huiskes, R., 2005b. Erratum to "Stresses in the local collagen network of articular cartilage: a poroviscoelastic fibril-reinforced finite element study" [Journal of Biomechanics

37 (2004) 357–366] and "A fibril-reinforced poroviscoelastic swelling model for articular cartil. J. Biomech. 38, 2138–2140. https://doi.org/10.1016/j.jbiomech.2005.04.024.

Wilson, W., van Donkelaar, C.C., van Rietbergen, B., Ito, K., Huiskes, R., 2004. Stresses in the local collagen network of articular cartilage: a poroviscoelastic fibril-reinforced finite element study. J. Biomech. 37, 357–366. https://doi.org/10.1016/S0021-9290(03)00267-7.

Wilusz, R.E., Sanchez-Adams, J., Guilak, F., 2014. The structure and function of the pericellular matrix of articular cartilage. Matrix Biol. 39C, 25–32. https://doi.org/10.1016/j.matbio.2014.08.009.

Wilusz, R.E., Zauscher, S., Guilak, F., 2013. Micromechanical mapping of early osteoarthritic changes in the pericellular matrix of human articular cartilage. Osteoarthr. Cartilage 21, 1895–1903. https://doi.org/10.1016/j.joca.2013.08.026.

Youn, I., Choi, J.B., Cao, L., Setton, L.A., Guilak, F., 2006. Zonal variations in the three-dimensional morphology of the chondron measured in situ using confocal microscopy. Osteoarthr. Cartilage 14, 889–897. https://doi.org/10.1016/j.joca.2006.02.017.

Zelenski, N.A., Leddy, H.A., Sanchez-Adams, J., Zhang, J., Bonaldo, P., Liedtke, W., Guilak, F., 2015. Collagen VI regulates pericellular matrix properties, chondrocyte swelling, and mechanotransduction in articular cartilage. Arthritis Rheumatol. (Hoboken, N.J.) 67, 1–26. https://doi.org/10.1002/art.39034.